Highlights

Electrochemical sensing of SARS-CoV-2 amplicons with PCB electrodes

M. S. Kumar, Ruchira Nandeshwar, Shailesh B. Lad, Kirti Megha, Maheshwar Mangat, Adrian Butterworth, Charles W. Knapp, Mara Knapp, Paul A. Hoskisson, Damion K. Corrigan, Andrew C. Ward, Kiran Kondabagil, Siddharth Tallur

- Adsorption of PCR amplicons electrochemically detected on low-cost PCB electrodes with methlyene blue (MB)
- Amplicon length and MB concentration are both critical to achieving linear sensor performance
- Detection of SARS-CoV-2 nucleocapsid gene amplicons from 10 pg/µl (1.7 fM)
- N1 fragment successfully amplified and detected in wastewater spiked with SARS-CoV-2 control RNA

Electrochemical sensing of SARS-CoV-2 amplicons with PCB electrodes

M. S. Kumar[a,*], Ruchira Nandeshwar[b,*], Shailesh B. Lad[a], Kirti Megha[a], Maheshwar Mangat[b], Adrian Butterworth[d], Charles W. Knapp[e], Mara Knapp[e], Paul A. Hoskisson[f], Damion K. Corrigan[d], Andrew C. Ward[e], Kiran Kondabagil[a,c,**], Siddharth Tallur[b,**]

[a]*Department of Biosciences and Bioengineering, IIT Bombay, Mumbai 400076, India*
[b]*Department of Electrical Engineering, IIT Bombay, Mumbai 400076, India*
[c]*Water Innovation Center: Technology, Research & Education (WICTRE), IIT Bombay, Mumbai 400076, India*
[d]*Department of Biomedical Engineering, University of Strathclyde, Glasgow G1 1XQ, Scotland*
[e]*Department of Civil and Environmental Engineering, University of Strathclyde, Glasgow G1 1XQ, Scotland*
[f]*Strathclyde Institute of Pharmacy and Biomedical Sciences, University of Strathclyde, Glasgow G1 1XQ, Scotland*

Abstract

We present a low-cost electrochemical DNA biosensor based on printed circuit board (PCB) electrodes for wastewater monitoring using portable PCR instruments, such as miniPCR®, without the requirement for qPCR reagents. PCB electrodes are attractive candidates for low-cost and sensitive DNA biosensors of relevance in a pandemic such as COVID-19, and facilitate the opportunity to map disease spread in Low-Middle Income Countries (LMICs) through monitoring of environmental samples such as wastewater.

*These authors contributed equally to this work.
**Corresponding authors
Email addresses: kirankondabagil@iitb.ac.in (Kiran Kondabagil), stallur@ee.iitb.ac.in (Siddharth Tallur)

The biosensor reported in this work is capable of detecting PCR amplicons through the intercalation of methylene blue (MB) with DNA, which increases the voltammogram peak current at the redox potential of MB. We describe how these changes are likely to result from the adsorption of MB-DNA complex on the electrode surface. The electrodes are reusable, easy to clean, do not undergo any surface modification and represent a cost-effective solution with long shelf-life. We also explore the impact that MB concentration and DNA length have upon our biosensor performance and provide insights useful to other investigators in the field. The sensor reported here is capable of detecting SARS-CoV-2 nucleocapsid gene amplicons at concentrations as low as 10 pg/µl (approximately 1.7 fM) and can detect nucleotides amplified after 10 PCR cycles. Furthermore, using the PCB electrode and approaches described here, SARS-CoV-2 amplicons were detected in simulated wastewater sample, by spiking wastewater collected from a sewage treatment plant in Mumbai, India with SARS-CoV-2 RNA.

Keywords: Methylene blue, DNA biosensor, PCB electrode, SARS-CoV-2, Wastewater epidemiology

1. Introduction

The COVID-19 pandemic has negatively impacted economies and communities globally since its spread in early 2020. One of the most effective ways to minimize and control the spread of the SARS-CoV-2 virus has been to limit close human contact and therefore social activity [1, 2]. Whilst this approach has been highly effective in reducing levels of spread, the overall economic and societal impact is extremely high. Furthermore, these measures

are difficult to meaningfully implement in many low-middle income countries (LMICs) where large proportions of the population are dependent upon informal labour for income and survival [3]. Another challenge in many LMICs is that the advanced laboratory facilities and skilled workforce required to achieve mass human testing cannot be implemented in the short timescales required to support contact tracing and thus reduce spread whilst allowing restrictions on person to person economic activities to take place. An alternative to molecular testing is the use of rapid, lateral flow immunochemistry testing, but these tests have lower sensitivity and specificity than gold standard qPCR testing [4, 5]. On the other hand, testing of wastewater for the presence of SARS-CoV-2 nucleic acid could be used as a surveillance tool to identify areas where the case numbers are likely to be increasing and therefore allow more targeted action to be taken to limit viral spread in specific regions.

Wastewater epidemiology has been widely recognized and researched as a tool for surveillance and management of the spread of SARS-CoV-2 [6–14]. Over the last year, several groups have used gold standard qPCR-based techniques in order to pilot surveillance methods globally including in India, Italy, and North America [15–18]. One potential problem is that qPCR still requires expensive laboratory infrastructure and skilled scientists or technicians to complete the assay. Furthermore, if resources are limited, testing of human samples would most likely take precedence over wastewater epidemiology surveillance. Therefore, lower cost, alternative approaches are required in order to support wastewater surveillance for SARS-CoV-2 in LMICs, thus supporting widespread adoption of a further tool in the fight against the

virus. One way to support this would be through the use of low-cost nucleic acid biosensors. In addition to serving as tools for data collection from populations which lack adequate access to healthcare and diagnostic testing, such technologies could potentially also serve as more accurate indicators of the scale of infection by including asymptomatic cases and recovered individuals not accounted in clinical tests, that continue to shed virions in feces.

The field of biosensors for nucleic acid and in particular DNA is well established (see [19] for a detailed review). Methylene Blue (MB) is a redox mediator that can be transduced with an electrochemical sensor. The intercalating properties of MB with DNA have resulted in its widespread use as a redox mediator in a range of electrochemical DNA sensor approaches [20–24]. These systems conventionally employ electrodes to immobilize the MB-DNA complex [24–28] or probe the DNA concentration in homogenous solution directly [29–33]. A common feature of all these studies is the prevention of DNA adsorption onto the electrode surface. In the case of gold electrodes, this has been achieved using an alkanethiol layer, such as 6-mercapto-1-heaxanol (MCH) [24, 34]. However, electrode modifications such as this can lead to more onerous electrode storage requirements prior to use. Also, the use of modification processes increases the complexity and thus production costs of the electrode. An alternative approach, is to use the ability of DNA to adsorb to the electrode surface as the basis for identification of PCR product.

The use of printed circuit boards (PCBs) conventionally used in the electronics manufacturing industry has been explored for Micro Total Analysis Systems (μTAS) platforms since early-1990s, however the focus for a large part of the previous three decades has been on demonstration of proof-of-

concept PCB based lab-on-chips, and not particularly on integration strategies and manufacturability. In recent times the cost of µTAS platforms has emerged as a significant technology driver, and therefore lab-on-PCB platforms are seeing renewed interest in the broad biosensors community [35–42]. Despite this, the technology is not as commonly adopted as screen printed electrodes, mainly due to challenges associated with impact of gold surface roughness on biorecognition element immobilization and the need for additional processing steps to ensure reliability due to the use of copper in PCBs, which is susceptible to corrosion and hampers electrochemical analysis [43, 44]. With suitable development, PCB electrode based electrochemical DNA sensors could be of great relevance in the COVID-19 pandemic [45] e.g. for mapping disease spread through monitoring of wastewater. In this paper, we build on the benefits of PCB based technologies and present a low-cost PCB electrode based electrochemical sensor for detection of SARS-CoV-2 PCR amplicons. The transduction mechanism is based on intercalation of MB with DNA, and change in current through voltammetry measurements resulting from adsorption of MB-DNA complex on the electrode surface. The PCB electrodes are manufactured using the conventional electroless nickel immersion gold (ENIG) process and do not undergo any surface modification. The electrodes thus present a cost-effective solution with long shelf-life, as they do not require any specific low-temperature storage conditions for normal operation, unlike electrodes with DNA immobilization or hybridization. The system design and approach can thus be implemented at very low cost with minimal resources, and provides a basis for a future low cost SARS-CoV-2 wastewater surveillance system (as illustrated in Figure 1(a)).

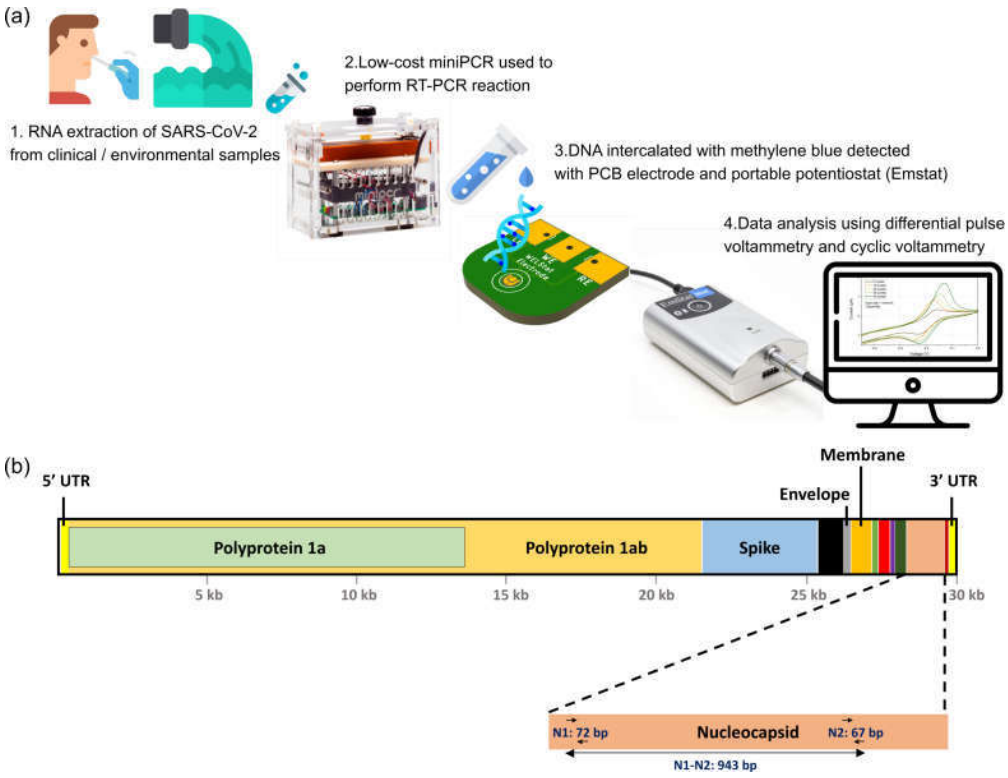

Figure 1: (a) SARS-CoV-2 nucleic acid detection workflow. RNA extracted from wastewater is amplified usinbg a low cost thermo cycler and then placed onto PCB electrodes. (b) Illustration of major protein coding genes of the SARS-CoV-2 coronavirus genome. The 943 bp N1-N2 fragment produced using N1 forward and N2 reverse primers used in this present study is also shown.

2. Materials and methods

2.1. Preparation of target amplicons

Control plasmid containing complete nucleocapsid (N) gene from SARS-CoV-2 isolate Wuhan-Hu-1 (GenBank: NC 045512.2; 2019-nCoV_N_Positive Control from IDT, supplied as 2×10^6 copies/µl) was used as template (10^2-10^6 copies per reaction) for amplifying the target fragment using mini8 PCR machine (miniPCR®) with the US CDC-recommended N1 and N2 forward and reverse primers (IDT). Fragments amplified included the N1 fragment (72 bp), and N1-N2 fragment (943 bp, using N1 forward and N2 reverse primers), as illustrated in Figure 1(b). In some instances, PCR reactions were stopped after fewer cycles (5, 10, 20, and 30 cycles) followed by a final extension of 10 min at 72 °C. The concentration of the PCR-amplified products was estimated using a Nanodrop spectrophotometer. For some measurements, the products were diluted (in Milli-Q water) to final concentrations of 10 pg/µl, 20 pg/µl, 50 pg/µl, 100 pg/µl, 150 pg/µl and 200 pg/µl. The template concentration chosen for amplification is 10^5 copies/µl unless otherwise mentioned. For measurements performed with DNA-MB complex, desired concentration of MB (5 µM, 10 µM, 50 µM or 100 µM) were added to the PCR product. The DNA-MB samples were incubated at room temperature for 1 h before performing measurements, to allow sufficient time for intercalation [21].

2.1.1. Generation of amplicons using different template concentrations

PCR using different template concentrations was performed to evaluate lower limit of sensing using PCB electrodes. 2019-nCoV_N_Positive Control from IDT was used as a template (10^2-10^5 copies per reaction) for amplifying

the target fragment using the mini8 thermal cycler (40 cycles) with CDC-recommended N1 forward and N2 reverse primers (IDT). The amplicons were visualized by agarose gel electrophoresis and ethidium bromide staining.

2.1.2. Preparation of intermediate PCR amplicons

2019-nCoV_N_Positive Control diluted to 10^5 copies/µl is used as template for PCR to amplify the 943 bp N product. The PCR reactions are stopped after 5, 10, 20, 30 and 40 cycles. Products obtained with <40 cycles undergo a final extension of 10 min at 72 °C in dry bath. The final amplified product (40 cycles) is left in mini8 for final extension. To verify the presence of PCR products, a 4 µl volume of each sample was electrophoresed on a 1 % agarose gel.

2.1.3. Generation of simulated wastewater sample for detection of SARS-CoV-2 amplicons

200 ml of grab wastewater samples were collected from a sewage treatment plant in Mumbai, India. The samples were heat-inactivated by incubating at 60 °C for 90 min, and the virus particles were concentrated using aluminum hydroxide adsorption method reported by Randazzo et al. [46]. Briefly, sample pH was adjusted to 6.0 before the addition of $AlCl_3$ solution. The pH was readjusted to 6.0 and the samples were incubated on a shaker at 150 rpm for 15 min at room temperature followed by centrifugation at 1700 g for 20 min to concentrate the viruses. The pellet was resuspended in 3 % beef extract and mixed slowly using a shaker at 150 rpm for 10 min at room temperature. The samples were then centrifuged at 1900 g for 30 min, and the pellet was resuspended in 1 ml of PBS. Total viral RNA was ex-

tracted from 150 µl of the resuspended pellet using the AllPrep PowerViral DNA/RNA kit (Qiagen, Germany) as per the manufacturer's instructions. RNA eluted in nuclease-free water was stored as aliquots at −80 °C. The presence of SARS-CoV-2 RNA was checked by performing RT-PCR with CDC-recommended N1 and N2 primers (IDT). As the sample did not contain any SARS-CoV-2 RNA, a simulated sample was generated by mixing the isolated total RNA with approximately 4.73×10^3 copies of the SARS-CoV-2 genomic RNA (VR-1986DTM, ATCC™). The RNA was reverse transcribed using a cDNA kit (Genetix Biotech Asia Pvt. Ltd., India) to amplify the 72 bp long N1 fragment.

2.2. Electrochemical biosensor

The PCB electrodes (Figure 2(a)) were designed using Autodesk EAGLE software and manufactured in conventional ENIG plating process (Circuit Systems (India) Ltd.). The manufacturing cost per electrode is approximately USD $0.55 (i.e. approximately INR ₹40). The electrodes were cleaned with an isopropyl alcohol (IPA) soaked lint-free wipe before each measurement. During each measurement, 5 µl of the sample to be tested was dispensed on the electrode. The electrode was then cleaned with a lint-free wipe dampened with IPA before dispensing the next sample. The voltammetry measurements were performed using Palmsens EmStat3 Blue potentiostat. The potentiostat configuration and data acquisition are performed using PSTrace software. Differential pulse voltammetry (DPV) measurements were performed using following settings: equilibration time = 8 s, voltage step = 3 mV, pulse voltage = 25 mV, pulse duration = 50 ms and scan rate = 20 mV/s. The potential (voltage) range is set as desired for each

measurement. Cyclic voltammetry (CV) measurements were performed at various scan rates using following settings: equilibration time = 8 s and voltage step = 3 mV. The voltage range and scan rate were set as desired for each measurement. The equilibration time is the time during which the first potential of the measurement is applied to the electrochemical cell without recording the current. This is done in order to exclude initial capacitive current from interfering with the Faradaic current to be measured. Peak heights for DPV peak current and cathodic peak current in CV voltammograms were obtained using PSTrace software. The values for peak height obtained from PSTrace software were used for preparation of graphs wherever peak current values are discussed.

3. Results and discussion

3.1. PCB electrodes can be reused multiple times after cleaning with IPA-wipe

The gold electrodes on the PCB were formed through an industry standard ENIG plating process, that results in a thin (<100 nm) gold layer on top of a thicker nickel layer (the nickel layer is designed to prevent diffusion of copper and gold layers). The nickel and copper layers underneath the gold are susceptible to corrosion and therefore incompatible with conventional gold electrode cleaning methods such as sulfuric acid potential cycling or piranha clean [47]. Since the samples to be measured comprise of organic compounds (MB and DNA), we clean the PCB electrodes with lint-free wipe dampened with IPA. Repeat measurements of 100 µM MB using this approach show that consistent peak DPV currents are observed (Figure 2(b)). Following measurements with 100 µM MB, no DPV peaks were

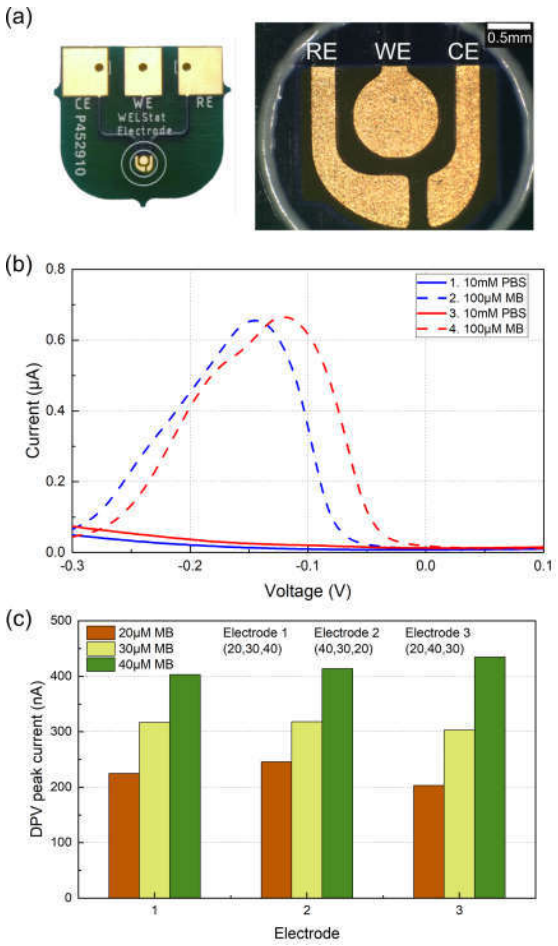

Figure 2: (a) Left - photograph of the PCB electrode used in this work. Right - optical micrograph of the PCB electrode showing reference electrode (RE), working electrode (WE), and counter electrode (CE), all formed with ENIG finish gold pads on the PCB. (b) The efficacy of cleaning process of the electrode is illustrated by measuring 10 mM PBS and 100 µM methylene blue (MB) successively in the order indicated in the figure legend, by wiping the electrode with IPA dampened wipe after each measurement. The first PBS measurement is performed to ensure there is no contamination on the electrode. No DPV peaks are seen in the third measurement performed with PBS, indicating that any MB adsorbed on the electrode is wiped away. (c) The peak current is proportional to the concentration of MB independent of the order of addition of MB solutions with different concentration (20 µM, 30 µM and 40 µM) on three electrodes (E1, E2, E3; order in which samples are dispensed is indicated in plot legend).

seen in the measurements performed with only PBS. This indicates that any residual MB on the electrode is wiped away through the cleaning process and provides confidence that the cleaning approach adopted does not negatively affect the thin gold layer on the electrode surface. DPV measurements were performed with various concentrations of MB (Figure 2(c)) on three electrodes, with samples dispensed sequentially in arbitrary order on each electrode (20 µM→30 µM→40 µM on electrode 1, 40 µM→30 µM→20 µM on electrode 2, and 20 µM→40 µM→30 µM on electrode 3). Overall, these results show that cleaning the electrodes with an IPA dampened wipe after measuring each sample is effective, based on the measurement repeatability seen on the three electrodes. Although the magnitude of the current was consistent across electrodes, it was found that the peak potential was not stable and varied across measurements (Figure 1 in Supplementary Information). The changes in the peak potential are likely to be caused by a number of issues, including the ratio of oxidized and reduced MB present, the subtle differences in dissolved species (solutes) between different samples, impurities on the surface of the reference electrode, and the use of gold reference electrode on the PCB instead of a stable reference such as Ag/AgCl. The electrode-to-electrode variation indicates that one cannot rely on a universal calibration curve when using multiple electrodes, and each electrode must be calibrated separately before use.

3.2. Longer DNA fragments result in peak current changes proportional to the concentration of DNA present

DPV voltammograms were obtained on PCB electrode for various DNA concentrations ranging from 10 pg/µl to 200 pg/µl complexed with 10 µM

MB. When the longer N1-N2 DNA amplicon (943 bp) was measured, we found that the peak DPV current increases with increasing DNA concentration, whereas the peak current for the shorter N1 fragment (72 bp) does not show any distinct trend (Figure 3(a)). To explore this further, DPV measurements were performed with 5 electrodes each for N1-N2 and N1 amplicons at different concentrations (Figure 3(b)). Linear regression shows that the longer N1-N2 fragment has larger sensitivity (0.605 nA/pg/µl) and better linearity ($R^2 = 0.88$) than the shorter N1 fragment (0.27 nA/pg/µl, $R^2 = 0.19$), indicating that the length of the DNA fragment has significant impact on sensor performance.

These results reveal that the amplicon length has a profound impact upon the linearity and therefore utility of the measurements performed. We believe these are attributed to intercalation of MB into the DNA and adsorption of the DNA onto the electrode surface. Other investigators have previously shown that the size of the oligonucleotide has a large impact on the adsorption at solid electrodes [48, 49]. The dependence of DNA-MB intercalation on DNA length and sequence has been reported previously [25, 50–52]. The intercalation of MB into the DNA base stack results in increase in current with increasing DNA concentration, since the DNA serves as a scaffold to bring the redox-active MB molecules into direct contact with the electrode surface, but does not participate directly in the electron-transfer event [53, 54]. The longer DNA fragments intercalate a greater quantity of MB and this in turn adsorbs to the unmodified gold electrode surface, resulting in a greater unit concentration of MB at the electrode surface compared to shorter DNA fragments.

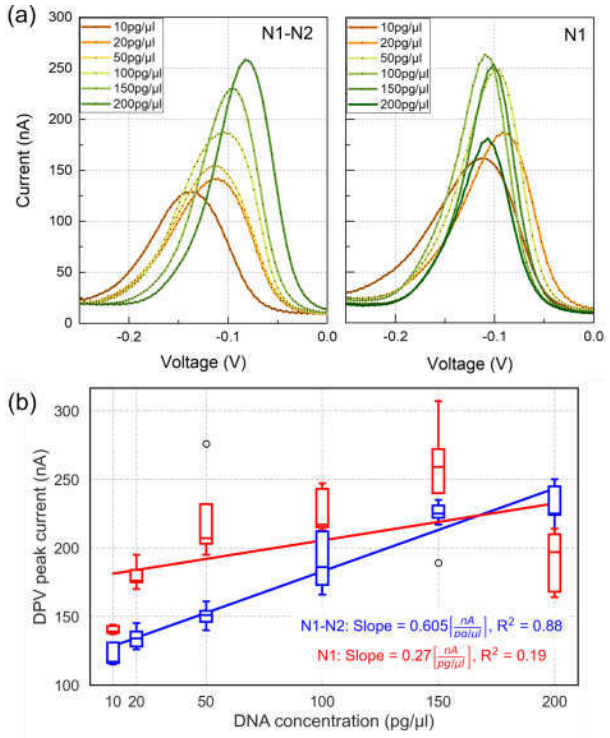

Figure 3: (a) DPV voltammograms obtained on PCB electrode for DNA-MB complex for various DNA concentrations complexed with 10 µM MB. Left - 943 bp PCR product (N1-N2); Right - 72 bp PCR product. (b) Linear regression of DPV measurements obtained with 5 electrodes each for N1-N2 and N1 indicate more linear sensor response for the longer N1-N2 fragment.

3.3. CV measurements indicate adsorption of DNA-MB complex at the electrode surface

Focusing upon the N1-N2 amplicon, we analyzed the electrochemical response of different samples to establish the role of DNA adsorption to the electrode surface. Firstly, we performed CV measurements at different scan rates for 50 µM MB (no DNA), and 100 pg/µl DNA (N1-N2) complexed with 50 µM MB (DNA+MB) (Figure 4(a)). As described above, the cathodic peak potential varies for both samples due to the use of gold reference electrode on the PCB instead of a stable reference such as Ag/AgCl. The cathodic and anodic peak currents increase with increasing scan rate as expected. When the logarithm of the cathodic peak current (expressed in nA) is examined with respect to the logarithm of the scan rate (expressed in mV/s), we observe a slope of approximately 1 (1.07 and 0.966 for MB and DNA-MB complex respectively). The linear trend is also clearly established with $R^2 \geq 0.98$ for MB and DNA-MB complex (Figure 4(b)). Electrochemically reversible electron transfer involving freely diffusing redox species correspond to $i_p \propto \nu^{0.5}$ (i.e. slope = 0.5 in $log(i_p) - log(\nu)$ plot), where i_p and ν denote cathodic peak current and scan rate respectively. In contrast, a slope of 1 (i.e. $i_p \propto \nu$) indicates that the current response is due to electrode-adsorbed species [55, 56], and thus points to adsorption of MB and DNA-MB complex on the gold electrodes. Adsorption of DNA-MB complex on the electrode leads to higher DPV current for higher DNA and MB concentrations.

3.4. Higher MB concentrations increase electrode sensitivity

To fully optimize the sensor performance, we explored the role MB concentration has upon the peak DPV current in response to changes in the

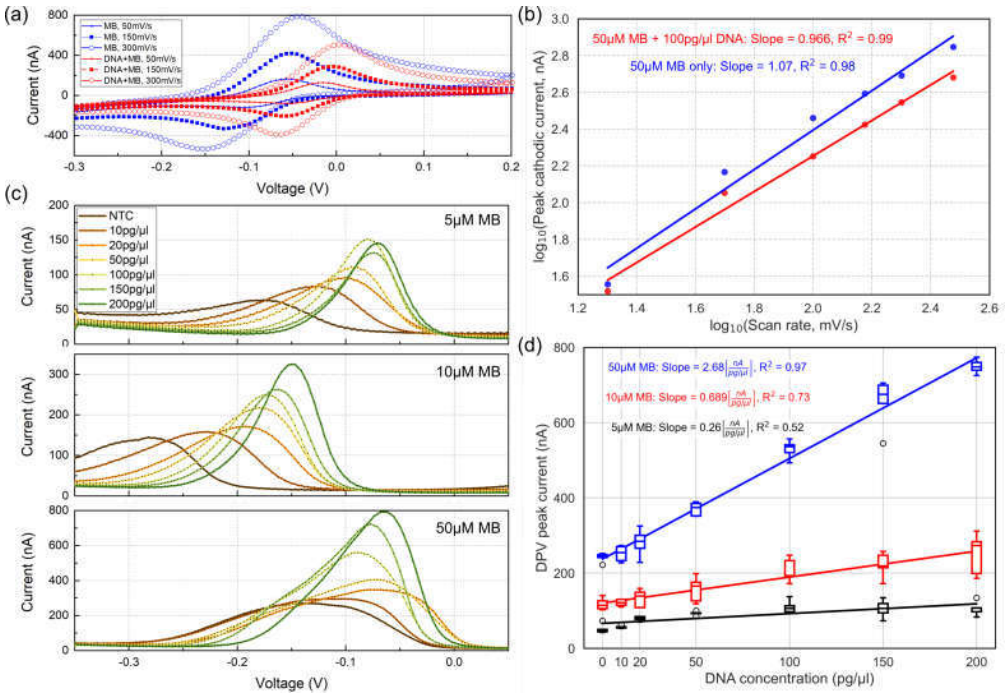

Figure 4: Electrochemical response of the sensor as a function of MB concentration. (a) Example CV measurements obtained at different scan rates for 50 µM MB only, and 100 pg/µl DNA (N1-N2) complex with 50 µM MB (DNA+MB). (b) Peak cathodic current variation with scan rate for MB only and DNA-MB complex displayed in log-log plot. The logarithm of peak cathodic current shows linear trend of variation with logarithm of scan rate, with slope ≈ 1, indicating that the current response is due to adsorption of MB and DNA-MB complex on the electrode surface. (c) DPV measurements obtained on PCB electrode for DNA(N1-N2)-MB complex for various concentrations of MB (5 µM, 10 µM, 50 µM) and DNA (ranging from 10 pg/µl to 200 pg/µl). (d) Linear regression of DPV measurements obtained with 5 electrodes each for 5 µM, 10 µM and 50 µM MB indicate that the sensor response is more linear for higher concentration of MB.

concentration of the N1-N2 amplicon. We performed DPV measurements on DNA-MB complexes with different concentrations of MB (5 µM, 10 µM, 50 µM) and DNA. The DNA concentration was varied from 10 pg/µl (approximately 1.7 fM, equivalent to 10^{12} copies/µl) to 200 pg/µl (Figure 4(c)). We also performed linear regression using DPV peak currents obtained with 5 electrodes each for 5 µM, 10 µM and 50 µM MB intercalated with DNA (Figure 4(d)). These results show that the sensitivity and linearity improve with increasing concentrations of MB (slope [nA/pg/µl] = 2.68, 0.689 and 0.26 for 50 µM, 10 µM and 5 µM MB respectively; R^2 = 0.97, 0.73 and 0.52 for 50 µM, 10 µM and 5 µM MB respectively). These results show that for our sensor design, the linearity and sensitivity are affected by the MB concentration. This has important implications for future studies and suggests that wide range of MB concentrations should be explored during the optimization stage of sensor development.

3.5. Long fragment PCR product is detectable after 10 *cycles with PCB electrodes*

Amplified products obtained using various template concentrations were visualized using agarose gel electrophoresis (Figure 5(a)). We found that the N1-N2 fragment (943 bp) is only visible for template concentrations of 10^4 and 10^5 copies/µl. After optimizing the PCB electrodes with respect to DNA length and MB concentration, we then explored the performance of the electrodes during PCR cycles. PCR product was visualized using agarose gel electrophoresis after 5, 10, 20, 30 and 40 cycles (Figure 5(b)). For intermediate PCR amplicons obtained with 10^5 copies/µl template, the amplified product is visible in agarose gel only beyond 20 cycles of PCR. In

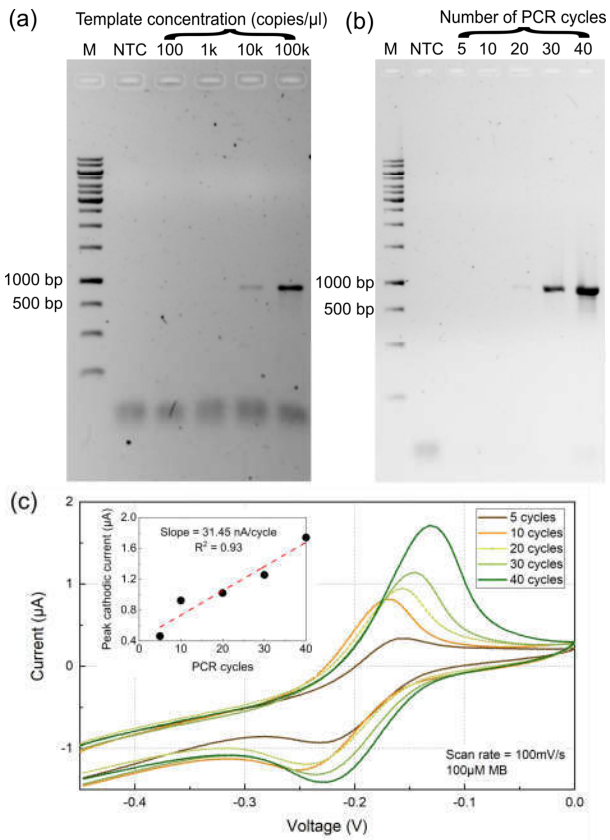

Figure 5: PCB electrode performace during intermediate PCR cycles. (a) Agarose gel showing the 2019-nCoV_N_Positive Control after 40 PCR cycles using the N1-N2 primers. The N1-N2 fragment is only visible with starting template concentrations of 10^4 and 10^5 copies/µl (M - Marker, NTC - Negative Control). (b) Agarose gel of PCR product following amplification of 10^5 copies template after fewer cycles. The amplified product is visible in agarose gel only beyond 20 cycles of PCR. (c) CV voltammograms obtained at 100 mV/s scan rate after adding 100 µM MB to the PCR products, showing that current response is proportional to the number of cycles.

contrast, the change in electrochemical sensor signal is clearly seen in the CV voltammogram performed at 100 mV/s scan rate after adding 100 µM MB to the PCR products (Figure 5(c)). Furthermore these results show a linear trend for variation in peak cathodic current with number of PCR cycles. The PCB electrodes are thus capable of discerning intermediate PCR products for as low as 10 PCR cycles (i.e. approximately 10^8 copies/µl), that are not visible in the agarose gel.

3.6. SARS-CoV-2 RNA can be isolated from wastewater and electrochemically detected using a low cost PCR machine and PCB electrode

We explored the utility of the system developed here with wastewater samples spiked with ATCC™ SARS-CoV-2 genomic RNA. While longer fragment amplicons appear to be better for MB intercalation and electrochemical detection, amplification efficiency of long fragments of SARS-CoV-2 RNA isolated from heterogeneous samples such as wastewater is challenging because RNA is prone to shearing and degradation during isolation. Importantly, we found that products longer than 500 bp could not be amplified efficiently. Considering these practical challenges associated with RNA isolation from heterogenous samples, PCR amplification and electrochemical sensing, it emerges that a multi-parameter optimization study is required to engineer a robust testing protocol. Though attempts were made to amplify the 943 bp N1-N2 fragment, we opted to focus upon the shorter 72 bp N1 region as this can be amplified more efficiently from wastewater (Figure 6(a)). It should be noted that when we work with heterogeneous environmental samples such as wastewater, it is possible that there may be non-specific amplification [57]. The band at approximately 20 bp in lanes NTC (no template

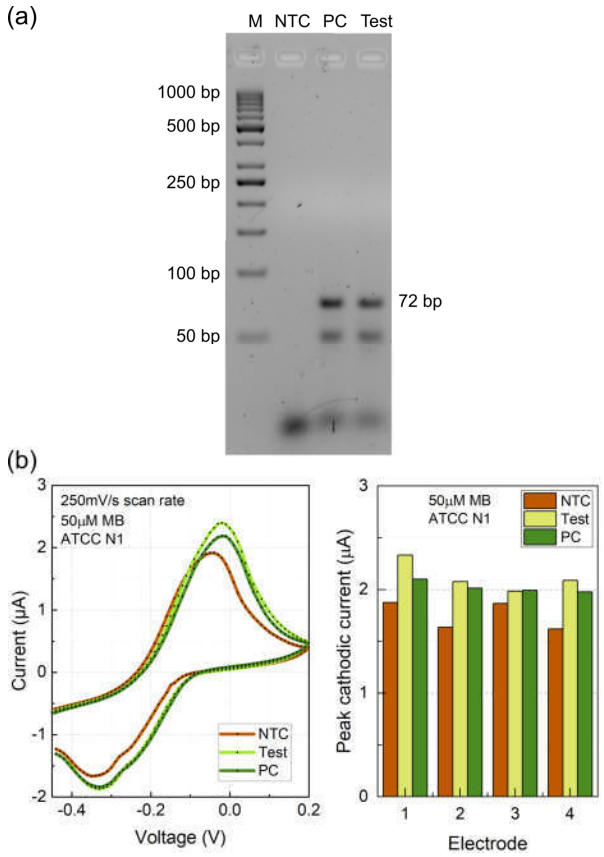

Figure 6: Detection of SARS-CoV-2 RNA spiked into wastewater using PCB electrodes. (a) Agarose gel showing PCR amplicons from a simulated wastewater sample containing SARS-CoV-2 RNA (M - Marker, NTC - Negative Control, PC - Positive Control, Test - Test Sample, SARS-CoV-2 RNA negative wastewater spiked with ATCC™ SARS-CoV-2 RNA as detailed in section 2.1.3). In addition to the expected band at 72 bp, we also found a band at approximately 50 bp in the positive control and sample. (b) (Left) Example CV voltammograms obtained on electrode 1, with 50 µM MB added to RT-PCR products. (Right) CV cathodic peak currents measured on 4 separate PCB electrodes. While there is large electrode-to-electrode variation, the PCB electrodes produce larger peak currents for test sample and PC than NTC.

control), PC (positive control), and Test corresponds to excess primers. After confirmation of PCR amplicons, we performed CV measurements using the PCB electrodes and found that a change in the peak current could be observed when the amplicons were present in the sample (Figure 6(b)). The negative control (NTC) also induces electrochemical sensor response due to adsorption of MB on the electrode, and therefore each electrode must be separately calibrated with NTC and PC samples in order to distinguish false positives from true positives. These results suggest that, with further development, the electrode system could be used in the field for determination of SARS-CoV-2 amplicons.

4. Conclusion

In this paper, we characterize a low-cost detection system for the identification of SARS-CoV-2 nucleic acid in wastewater. Our approach takes advantage of existing primer sets, and uses a commercially available low-cost thermocycler to reverse transcribe and amplify key regions. Using this sensor system, we report that it is possible to identify the presence of SARS-CoV-2 in wastewater. We showed that the peak DPV current is proportional to the DNA concentration due to the adsorption of DNA-MB complex on the electrode. We also show that the electrochemical sensitivity is strongly determined by concentration of MB and the length of the DNA fragment. The platform presented in this work is a cost-effective electrochemical sensing solution, with manufacturing costing as low as USD $0.55 (INR ₹40) per electrode for quantities of 100. Unlike real-time PCR (qPCR) techniques, this platform does not require expensive reagents or instrumentation, thus

further boosting the cost-effectiveness of this solution. The electrodes are also easily cleaned using a lint-free wipe dampened with IPA and are reusable. Furthermore, the electrodes do not undergo any surface modification and thus have long shelf-life. Our future work will focus upon identifying optimal primers for both PCR amplification and electrochemical sensing, integrating this assay with on-board thermocycling and electrochemical measurement, and exploring methods for enhanced stability of the reference electrode to achieve redox peaks at consistent potentials.

Acknowledgments

M.S.K. acknowledges Council of Scientific and Industrial Research (CSIR) - University Grants Commission (UGC), Ministry of Education (formerly Ministry of Human Resource Development), Government of India, for supporting his Ph.D. scholarship. R.N. acknowledges Ministry of Education (formerly Ministry of Human Resource Development), Government of India, for supporting her Ph.D. scholarship. This work was supported by a grant from the Scottish Funding Council (SFC) Global Challenges Research Fund (GCRF) COVID-19 Response Fund, grant SFC/AN/14/2019. The electrochemical sensor characterization was performed at the Wadhwani Electronics Lab (WEL), supported by a grant from Wadhwani Charitable Foundation (WCF). Research in KK lab is supported by the Department of Science and Technology (DST), Ministry of Science and Technology, Government of India, grant DST/TM/WT1/WIC/2K17/100(C). The authors thank Mr. Mahesh Bhaganagare, Mrs. Madhumita P. Date and other staff at the Wadhwani Electronics Lab (WEL), IIT Bombay, for assistance in conducting prelimi-

nary experiments.

Author contributions statement

M. S. Kumar: Conceptualization, Methodology, Investigation, Formal analysis, Visualization, Validation, Writing - Original Draft; **Ruchira Nandeshwar:** Conceptualization, Methodology, Investigation, Formal analysis, Visualization, Writing - Original Draft; **Shailesh B. Lad:** Conceptualization, Methodology, Investigation, Writing - Review & Editing; **Kirti Megha:** Conceptualization, Methodology, Investigation, Writing - Review & Editing; **Maheshwar Mangat:** Conceptualization, Methodology, Investigation, Validation; **Adrian Butterworth:** Conceptualization, Funding acquisition, Writing - Review & Editing; **Charles W. Knapp:** Conceptualization, Funding acquisition, Writing - Review & Editing; **Mara Knapp:** Conceptualization, Funding acquisition, Writing - Review & Editing; **Paul A. Hoskisson:** Conceptualization, Funding acquisition, Writing - Review & Editing; **Damion K. Corrigan:** Conceptualization, Funding acquisition, Writing - Review & Editing; **Andrew C. Ward:** Conceptualization, Methodology, Supervision, Funding acquisition, Project administration, Investigation, Formal analysis, Writing - Review & Editing; **Kiran Kondabagil:** Conceptualization, Methodology, Supervision, Funding acquisition, Project administration, Formal analysis, Writing - Original Draft, Writing - Review & Editing; **Siddharth Tallur:** Conceptualization, Methodology, Supervision, Funding acquisition, Project administration, Investigation, Formal analysis, Writing - Original Draft, Writing - Review & Editing

Declaration of interest

The authors declare that they have no known competing financial interests or personal relationships that could have appeared to influence the work reported in this paper.

References

[1] E. Janik, M. Bartos, M. Niemcewicz, L. Gorniak, M. Bijak, SARS-CoV-2: Outline, Prevention, and Decontamination, Pathogens 10 (2021) 114.

[2] M. Mofijur, I. R. Fattah, M. A. Alam, A. S. Islam, H. C. Ong, S. A. Rahman, G. Najafi, S. Ahmed, M. A. Uddin, T. Mahlia, Impact of covid-19 on the social, economic, environmental and energy domains: Lessons learnt from a global pandemic, Sustainable production and consumption 26 (2021) 343–359.

[3] I. L. Organization, ILO Monitor: Covid-19 and the world of work, 2020.

[4] S. Alpdagtas, E. Ilhan, E. Uysal, M. Sengor, C. B. Ustundag, O. Gunduz, Evaluation of current diagnostic methods for COVID-19, APL bioengineering 4 (2020) 041506.

[5] J. Watson, P. F. Whiting, J. E. Brush, Interpreting a covid-19 test result, Bmj 369 (2020).

[6] W. Lodder, A. M. de Roda Husman, SARS-CoV-2 in wastewater: potential health risk, but also data source, The lancet Gastroenterology & hepatology 5 (2020) 533–534.

[7] D. A. Larsen, K. R. Wigginton, Tracking COVID-19 with wastewater, Nature Biotechnology 38 (2020) 1151–1153.

[8] D. Barceló, Wastewater-Based Epidemiology to monitor COVID-19 outbreak: Present and future diagnostic methods to be in your radar, Case Studies in Chemical and Environmental Engineering 2 (2020) 100042.

[9] P. Foladori, F. Cutrupi, N. Segata, S. Manara, F. Pinto, F. Malpei, L. Bruni, G. La Rosa, SARS-CoV-2 from faeces to wastewater treatment: what do we know? A review, Science of the Total Environment 743 (2020) 140444.

[10] D. Polo, M. Quintela-Baluja, A. Corbishley, D. L. Jones, A. C. Singer, D. W. Graham, J. L. Romalde, Making waves: Wastewater-based epidemiology for COVID-19–approaches and challenges for surveillance and prediction, Water Research 186 (2020) 116404.

[11] T. Zuo, Q. Liu, F. Zhang, G. C.-Y. Lui, E. Y. Tso, Y. K. Yeoh, Z. Chen, S. S. Boon, F. K. Chan, P. K. Chan, et al., Depicting SARS-CoV-2 faecal viral activity in association with gut microbiota composition in patients with COVID-19, Gut 70 (2021) 276–284.

[12] W. Lin, Z. Xie, Y. Li, L. Li, C. Wen, Y. Cao, X. Chen, X. Ou, F. Hu, F. Li, et al., Association between detectable SARS-COV-2 RNA in anal swabs and disease severity in patients with coronavirus disease 2019, Journal of medical virology 93 (2021) 794–802.

[13] J. Liu, Y. Xiao, Y. Shen, C. Shi, Y. Chen, P. Shi, Y. Gao, Y. Wang, B. Lu, Detection of SARS-CoV-2 by RT-PCR in anal from patients

who have recovered from coronavirus disease 2019, Journal of medical virology 92 (2020) 1769–1771.

[14] Y. Tian, L. Rong, W. Nian, Y. He, Gastrointestinal features in COVID-19 and the possibility of faecal transmission, Alimentary pharmacology & therapeutics 51 (2020) 843–851.

[15] S. P. Sherchan, S. Shahin, L. M. Ward, S. Tandukar, T. G. Aw, B. Schmitz, W. Ahmed, M. Kitajima, First detection of SARS-CoV-2 RNA in wastewater in North America: a study in Louisiana, USA, Science of The Total Environment 743 (2020) 140621.

[16] E. Haramoto, B. Malla, O. Thakali, M. Kitajima, First environmental surveillance for the presence of SARS-CoV-2 RNA in wastewater and river water in Japan, Science of The Total Environment 737 (2020) 140405.

[17] S. G. Rimoldi, F. Stefani, A. Gigantiello, S. Polesello, F. Comandatore, D. Mileto, M. Maresca, C. Longobardi, A. Mancon, F. Romeri, et al., Presence and infectivity of SARS-CoV-2 virus in wastewaters and rivers, Science of the Total Environment 744 (2020) 140911.

[18] M. Kumar, A. K. Patel, A. V. Shah, J. Raval, N. Rajpara, M. Joshi, C. G. Joshi, First proof of the capability of wastewater surveillance for COVID-19 in India through detection of genetic material of SARS-CoV-2, Science of The Total Environment 746 (2020) 141326.

[19] E. Palecek, M. Bartosik, Electrochemistry of nucleic acids, Chemical Reviews 112 (2012) 3427–3481.

[20] A. Tani, A. J. Thomson, J. N. Butt, Methylene blue as an electrochemical discriminator of single-and double-stranded oligonucleotides immobilised on gold substrates, Analyst 126 (2001) 1756–1759.

[21] E. L. Wong, P. Erohkin, J. J. Gooding, A comparison of cationic and anionic intercalators for the electrochemical transduction of DNA hybridization via long range electron transfer, Electrochemistry communications 6 (2004) 648–654.

[22] E. L. Wong, J. J. Gooding, Charge transfer through DNA: a selective electrochemical DNA biosensor, Analytical chemistry 78 (2006) 2138–2144.

[23] T. H. Fang, N. Ramalingam, D. Xian-Dui, T. S. Ngin, Z. Xianting, A. T. L. Kuan, E. Y. P. Huat, G. Hai-Qing, Real-time pcr microfluidic devices with concurrent electrochemical detection, Biosensors and Bioelectronics 24 (2009) 2131–2136.

[24] B. Y. Won, S. Shin, S. Baek, Y. L. Jung, T. Li, S. C. Shin, D.-Y. Cho, S. B. Lee, H. G. Park, Investigation of the signaling mechanism and verification of the performance of an electrochemical real-time PCR system based on the interaction of methylene blue with DNA, Analyst 136 (2011) 1573–1579.

[25] E. Farjami, L. Clima, K. V. Gothelf, E. E. Ferapontova, DNA interactions with a methylene blue redox indicator depend on the DNA length and are sequence specific, Analyst 135 (2010) 1443–1448.

[26] H.-Y. Tseng, V. Adamik, J. Parsons, S.-S. Lan, S. Malfesi, J. Lum, L. Shannon, B. Gray, Development of an electrochemical biosensor array for quantitative polymerase chain reaction utilizing three-metal printed circuit board technology, Sensors and Actuators B: Chemical 204 (2014) 459–466.

[27] L. Lu, J. C. Si, Z. F. Gao, Y. Zhang, J. L. Lei, H. Q. Luo, N. B. Li, Highly selective and sensitive electrochemical biosensor for ATP based on the dual strategy integrating the cofactor-dependent enzymatic ligation reaction with self-cleaving DNAzyme-amplified electrochemical detection, Biosensors and Bioelectronics 63 (2015) 14–20.

[28] S. Cinti, E. Proietti, F. Casotto, D. Moscone, F. Arduini, Paper-based strips for the electrochemical detection of single and double stranded DNA, Analytical chemistry 90 (2018) 13680–13686.

[29] T. Deféver, M. Druet, D. Evrard, D. Marchal, B. Limoges, Real-time electrochemical PCR with a DNA intercalating redox probe, Analytical chemistry 83 (2011) 1815–1821.

[30] F.-T. Zhang, J. Nie, D.-W. Zhang, J.-T. Chen, Y.-L. Zhou, X.-X. Zhang, Methylene blue as a G-quadruplex binding probe for label-free homogeneous electrochemical biosensing, Analytical chemistry 86 (2014) 9489–9495.

[31] F.-T. Zhang, L.-Y. Cai, Y.-L. Zhou, X.-X. Zhang, Immobilization-free DNA-based homogeneous electrochemical biosensors, TrAC Trends in Analytical Chemistry 85 (2016) 17–32.

[32] A. Martin, K. B. Grant, F. Stressmann, J.-M. Ghigo, D. Marchal, B. Limoges, Ultimate single-copy DNA detection using real-time electrochemical LAMP, Acs Sensors 1 (2016) 904–912.

[33] E. Nunez-Bajo, A. S. P. Collins, M. Kasimatis, Y. Cotur, T. Asfour, U. Tanriverdi, M. Grell, M. Kaisti, G. Senesi, K. Stevenson, et al., Disposable silicon-based all-in-one micro-qPCR for rapid on-site detection of pathogens, Nature communications 11 (2020) 1–10.

[34] T. M. Herne, M. J. Tarlov, Characterization of DNA probes immobilized on gold surfaces, Journal of the American Chemical Society 119 (1997) 8916–8920.

[35] D. Moschou, A. Tserepi, The lab-on-PCB approach: tackling the μTAS commercial upscaling bottleneck, Lab on a Chip 17 (2017) 1388–1405.

[36] B. B. Narakathu, S. G. R. Avuthu, A. Eshkeiti, S. Emamian, M. Z. Atashbar, Development of a microfluidic sensing platform by integrating PCB technology and inkjet printing process, IEEE Sensors Journal 15 (2015) 6374–6380.

[37] F. Güth, P. Arki, T. Löher, A. Ostmann, Y. Joseph, Electrochemical sensors based on printed circuit board technologies, Procedia Engineering 168 (2016) 452–455.

[38] F. T. Moreira, M. J. M. Ferreira, J. R. Puga, M. G. F. Sales, Screen-printed electrode produced by printed-circuit board technology: Application to cancer biomarker detection by means of plastic antibody as

sensing material, Sensors and Actuators B: Chemical 223 (2016) 927–935.

[39] D. Evans, K. I. Papadimitriou, N. Vasilakis, P. Pantelidis, P. Kelleher, H. Morgan, T. Prodromakis, A novel microfluidic point-of-care biosensor system on printed circuit board for cytokine detection, Sensors 18 (2018) 4011.

[40] K. Tsougeni, A. Kastania, G. Kaprou, M. Eck, G. Jobst, P. Petrou, S. Kakabakos, D. Mastellos, E. Gogolides, A. Tserepi, A modular integrated lab-on-a-chip platform for fast and highly efficient sample preparation for foodborne pathogen screening, Sensors and Actuators B: Chemical 288 (2019) 171–179.

[41] H. Shamkhalichenar, C. J. Bueche, J.-W. Choi, Printed Circuit Board (PCB) Technology for Electrochemical Sensors and Sensing Platforms, Biosensors 10 (2020) 159.

[42] H. Zhu, Z. Fohlerová, J. Pekárek, E. Basova, P. Neužil, Recent advances in lab-on-a-chip technologies for viral diagnosis, Biosensors and Bioelectronics 153 (2020) 112041.

[43] G. Dutta, A. Regoutz, D. Moschou, Commercially fabricated printed circuit board sensing electrodes for biomarker electrochemical detection: The importance of electrode surface characteristics in sensor performance, in: Multidisciplinary Digital Publishing Institute Proceedings, volume 2, 2018, p. 741.

[44] D. Moschou, T. Trantidou, A. Regoutz, D. Carta, H. Morgan, T. Prodromakis, Surface and electrical characterization of Ag/AgCl pseudo-reference electrodes manufactured with commercially available PCB technologies, Sensors 15 (2015) 18102–18113.

[45] N. Bhalla, Y. Pan, Z. Yang, A. F. Payam, Opportunities and challenges for biosensors and nanoscale analytical tools for pandemics: COVID-19, ACS Nano 14 (2020) 7783–7807.

[46] W. Randazzo, P. Truchado, E. Cuevas-Ferrando, P. Simón, A. Allende, G. Sánchez, SARS-CoV-2 RNA in wastewater anticipated COVID-19 occurrence in a low prevalence area, Water research 181 (2020) 115942.

[47] L. M. Fischer, M. Tenje, A. R. Heiskanen, N. Masuda, J. Castillo, A. Bentien, J. Émneus, M. H. Jakobsen, A. Boisen, Gold cleaning methods for electrochemical detection applications, Microelectronic engineering 86 (2009) 1282–1285.

[48] A. Steel, R. Levicky, T. Herne, M. J. Tarlov, Immobilization of nucleic acids at solid surfaces: effect of oligonucleotide length on layer assembly, Biophysical journal 79 (2000) 975–981.

[49] M. Pedano, G. Rivas, Immobilization of dna on glassy carbon electrodes for the development of affinity biosensors, Biosensors and Bioelectronics 18 (2003) 269–277.

[50] R. García-González, A. Costa-García, M. T. Fernández-Abedul, Methylene blue covalently attached to single stranded DNA as electroactive

label for potential bioassays, Sensors and Actuators B: Chemical 191 (2014) 784–790.

[51] C. Li, X. Chen, N. Wang, B. Zhang, An ultrasensitive and label-free electrochemical DNA biosensor for detection of DNase I activity, RSC advances 7 (2017) 21666–21670.

[52] W. Yang, M. Ozsoz, D. B. Hibbert, J. J. Gooding, Evidence for the direct interaction between methylene blue and guanine bases using DNA-modified carbon paste electrodes, Electroanalysis: An International Journal Devoted to Fundamental and Practical Aspects of Electroanalysis 14 (2002) 1299–1302.

[53] C. G. Pheeney, J. K. Barton, DNA electrochemistry with tethered methylene blue, Langmuir 28 (2012) 7063–7070.

[54] A. L. Furst, M. G. Hill, J. K. Barton, Electrocatalysis in DNA sensors, Polyhedron 84 (2014) 150–159.

[55] N. Elgrishi, K. J. Rountree, B. D. McCarthy, E. S. Rountree, T. T. Eisenhart, J. L. Dempsey, A practical beginner's guide to cyclic voltammetry, Journal of chemical education 95 (2018) 197–206.

[56] A. J. Bard, L. R. Faulkner, Electrochemical methods: Fundamentals and applications, Wiley New York, 2001.

[57] K. Megha, S. B. Lad, K. Kondabagil, Detection of SARS-CoV-2 in wastewater: Less than what meets the eye?, Communicated (2021).